New lifetime measurements for the lowest quadrupole states in ^{20,22}Ne and possible explanations of the high collectivity of the depopulating $E2$ transitions

P. Petkov,[1,2] C. Müller-Gatermann,[2] D. Werner,[2] A. Dewald,[2] A. Blazhev,[2] C. Fransen,[2] J. Jolie,[2] S. Ohkubo,[3] and K. O. Zell[2]

[1] *"Horia Hulubei" National Institute for Physics and Nuclear Engineering, R-76900 Bucharest-Măgurele, Romania*

[2] *Institut für Kernphysik der Universität zu Köln, D-50937 Cologne, Germany*

[3] *Research Center for Nuclear Physics, Osaka University, Ibaraki, Osaka 567-0047, Japan*

(Received 13 March 2019; revised manuscript received 5 June 2019; published 9 August 2019)

Shell model and multiparticle-multihole configuration-mixing calculations indicate a missing quadrupole collectivity needed to explain the transition strengths in the even-even Ne isotopes. Even with a significant scaling of the effective charges all details of the data cannot be reproduced. The effect is very pronounced in ^{20,22}Ne. Therefore new lifetime measurements in these nuclei were undertaken by us with the Doppler-shift attenuation method to recheck experimentally earlier findings. They confirmed the previous result in the case of ^{20}Ne while in ^{22}Ne the 2_1^+ level lifetime was found to be shorter by 43%. It turned out that in the latter nucleus the lifetime of the 4_1^+ level also has to be corrected. The $B(E2; 2_1^+ \rightarrow 0_1^+)$ reduced transition strengths derived from the newly determined lifetimes as well as those for the heavier Ne isotopes are reasonably described by involving a mixing of α-cluster states of, e.g., the type $\alpha \otimes$ 16O with normal, nearly spherical states. An extended version of the coupled-cluster effective interaction method published earlier describes well the spin dependence of the $B(E2)$'s in ^{20}Ne.

DOI: 10.1103/PhysRevC.100.024312

I. INTRODUCTION

Light nuclei are natural laboratories for investigating and trying to find solutions of the nuclear many-body quantum problem because of the relatively small number of particles involved [1–3]. Precise experimental data are of primordial importance for providing theorists with reliable benchmarks for their calculations. While excitation energies and spins of the lowest levels in these nuclei are well known, the lifetime data, extremely closely associated with the determination of absolute transition strengths, are not really reliable in all cases. For example, such conclusions were made in our very recent work [4]. There, it was shown that the Blaugrund approximation [5] could have led to some imprecise lifetime determinations in the past when using the Doppler-shift attenuation method (DSAM). Comparison with Monte Carlo simulations of the slowing-down process [6,7] show that there is not an easy way to judge on the reliability of old lifetime data. However, discrepancies and deviations can be due not only to the above-quoted approximation, which may work quite nicely in some cases, but also due to the use of wrong stopping powers and imprecisely taking into account the feeding from higher-lying levels [4]. From this point of view, a special interest represent the nuclei ^{20,22}Ne where the $2_1^+ \rightarrow 0_1^+$ transitions are characterized by very large $B(E2)$ values, which are difficult to be accommodated within systematic shell model or configuration mixing calculations (see, e.g., Fig. 6 in Ref. [8]). That is why it is important to revisit experimentally the lifetimes of the first 2^+ states in these two nuclei.

The history of the theoretical investigation of ^{20}Ne begins with the work of Elliott [9] exemplifying its excitation-energy spectrum as an example of the SU(3) symmetry in the shell model closely associated with deformed nuclei. The large $B(E2)$ transition strengths found later experimentally in the ground band of this nucleus confirmed its special place on the nuclear map. Due to the relatively small number of nucleons building up ^{20}Ne, the latter became an application target for different variants of the shell model [10–12], and later of multiparticle-multihole configuration mixing calculations [8,13] until the emergence of methods based on first principles and *ab initio* approaches as in Refs. [14,15]. We just quote only few and relatively recent calculations concentrating on low-lying nuclear structure available for ^{20,22}Ne and heavier Ne isotopes among the multitude of studies (for example, the NNDC keeps a record of more than 2500 papers dedicated to ^{20}Ne in the beginning of 2019). In the following discussion, the comparison of these calculations with the experimental data including the new ones will point to their success, in general, and to some especially nice descriptions.

On the other hand, another approach to treat theoretically the many-body problem is based on the consideration of the nucleus as composed from clusters, in the simplest case α particles. At the price paid for some phenomenology, this approach obviously reduces the number of considered constituents and has many experimental confirmations of its approximate validity, especially in light nuclei [16,17]. Only recently [18] α-cluster states have been found in nuclei as heavy as ^{212}Po where an α particle is coupled to the doubly magic ^{208}Pb core. These states decay via very strong $E1$ transitions because of the induced electric dipole moment in this mass-asymmetric composite system. Such clustering was investigated before the work [18] in Ref. [19], and later in Ref. [20].

More recently [21], states characterized by enhanced decaying $E1$ strength have been interpreted within the framework of the *spdf* interacting Boson model providing further evidence for the formation of α clusters in medium-mass nuclei. Therefore apart from the shell model, we employ for the interpretation of the data also models based on the consideration of the structure of ^{20,22}Ne as including mixing between $\alpha \otimes {}^{16}$O and $\alpha \otimes {}^{18}$O cluster states and spherical shell-model states (see, e.g., Refs. [22–24], also the Erratum [25]).

Experimentally, ^{20}Ne was thoroughly investigated in the past. Lifetimes of excited levels were measured using different reactions and the Doppler-shift attenuation method in Refs. [26–32,35,36]. The results all over the years are summarized in Ref. [33]. In the overwhelming majority of these works the strong collectivity of the yrast $E2$ transitions in ^{20}Ne is readily established, also at the level of quantitative agreement between the different data sets. Lifetimes in ^{22}Ne were measured in Refs. [28,34–46]. Here both the recoil-distance Doppler-shift and the Doppler-shift attenuation method were used. A compilation of the results can be found in Ref. [66]. In all these experiments, no gates on feeding transitions were employed, which may lead to problems associated with the unknown or side feeding. Very often, if the latter is not taken into account correctly, the result is a lifetime that is longer than the real one.

The paper is built as follows. First, the experiments performed are presented. A special attention is paid to the measurement of the stopping powers of the recoiling reaction products in the target and stopper. After that, the methods employed for the data analysis are described followed by the presentation of the results on lifetimes and transition strengths. Next, a discussion of the results in the framework of different theoretical models is made with conclusions at the end.

II. EXPERIMENTS

A. DSAM measurement for ^{20,22}Ne

The DSAM experiment on ^{20}Ne was performed at the FN tandem accelerator of the University of Cologne, Germany, using the setup of the Cologne coincidence plunger [47]. Excited states in ^{20}Ne were populated by a fusion evaporation reaction and a ^{16}O beam at energies of $E = 30$, 33, 36, and 38 MeV. The target was made of ^{9}Be with a thickness of 0.9 mg/cm^2 and $^{\text{nat}}$Mg was evaporated onto the target with a thickness of 2.7 mg/cm^2 to stop the evaporation residues. Deexciting γ rays were detected by twelve high-purity germanium (HPGe) detectors. These were mounted in three rings: one HPGe detector was positioned under an angle of 0° (ring 0), six were positioned under an angle of 45°, and five under an angle of 142.3° (ring 2) with respect to the beam direction. The distance between the target and the detectors was about 10 cm leading to a γ-ray efficiency of 1.8% at 1.3 MeV. Data were collected on average for 12 h per beam energy at a beam current of 3 pnA. The same setup with the same target was used for the experiment on ^{22}Ne. The beam was changed to ^{18}O at an energy of 33 MeV. Data of ^{22}Ne were taken for 6 h using the same outgoing αn-reaction channel.

B. Determination of the stopping powers of ^{20,22}Ne ions in the target and stopper materials

To determine the stopping powers used in the analysis experimentally another setup at a different accelerator of the University of Cologne was used. The accelerator [48] is also a Tandem accelerator with a maximum terminal voltage of 6 MV and typically used for accelerator mass spectrometry (AMS). Since neon does not form a negative ion, the neighboring ^{19}F and ^{23}Na isotopes were used as beams and an interpolation applied for the corresponding Ne nuclei. The setup consisted of a silicon detector to measure the energy of the ions and a retractable target ladder with a Faraday cup in front of the detector. The beams with ten different energies ranging from 6–30 MeV were used for energy calibration of the detector together with a ^{241}Am, ^{244}Cm, ^{239}Pu triple-α source. A 0.92(9) mg/cm^2 Be- foil and a 0.26(3) mg/cm^2 Mg were inserted and the energy losses in the foils were measured. In the case of the Be target only five initial energies were used, because of the higher energy loss in the thick target. X-Y slits in front of the target ladder provided a well-focused beam and an aperture with 2 mm in diameter on the detector guaranteed that angular straggling is neglectable. The data were compared to the tables of Northcliffe and Schilling and the stopping powers used by SRIM. All deviations were within 10% experimental error. The same variation is often included in the lifetime determination as a systematic error due to the incomplete knowledge of stopping powers. In Fig. 1 a comparison of the interpolated experimental data and the literature values by Northcliffe and Schilling and the code SRIM is presented showing the energy loss in Mg.

III. DATA ANALYSIS AND RESULTS

A. Description of the deceleration process and general framework of the analysis

For the description of the slowing-down process via Monte Carlo methods [i.e., for the calculation of the matrix $P_\theta(t, v_\theta)$] we used a modified version of the computer code DESASTOP [7,51] by Winter (cf. also Ref. [52]). The kinematics of the reactions used were also taken into account in the Monte Carlo simulation. The electronic stopping power for ^{20,22}Ne ions in Be and Mg was determined as described in the section dedicated to the experiments. The nuclear stopping power, which is due to the interaction with the atoms of the medium as a whole, was taken into account according to the LSS theory [53] and the parametrization of the universal scattering function for a Thomas-Fermi potential given in Ref. [6]. To correct for the effect of microchanneling in the stopping medium, the nuclear stopping power was reduced by a factor $f_n = 0.7$ (cf. Refs. [54,55] for more details).

The lifetime determination in the framework of the Doppler-shift attenuation method (DSAM) is based on the time correlation between the slowing down of the recoiling ion and the decay of the nuclear level of interest (cf., e.g., Ref. [56]). The latter should occur on the same time scale as the slowing down. The difference between the expected lifetimes in the two experiments led to the use of two different variants for data analysis. For the 2_1^+ level in ^{20}Ne, gates on

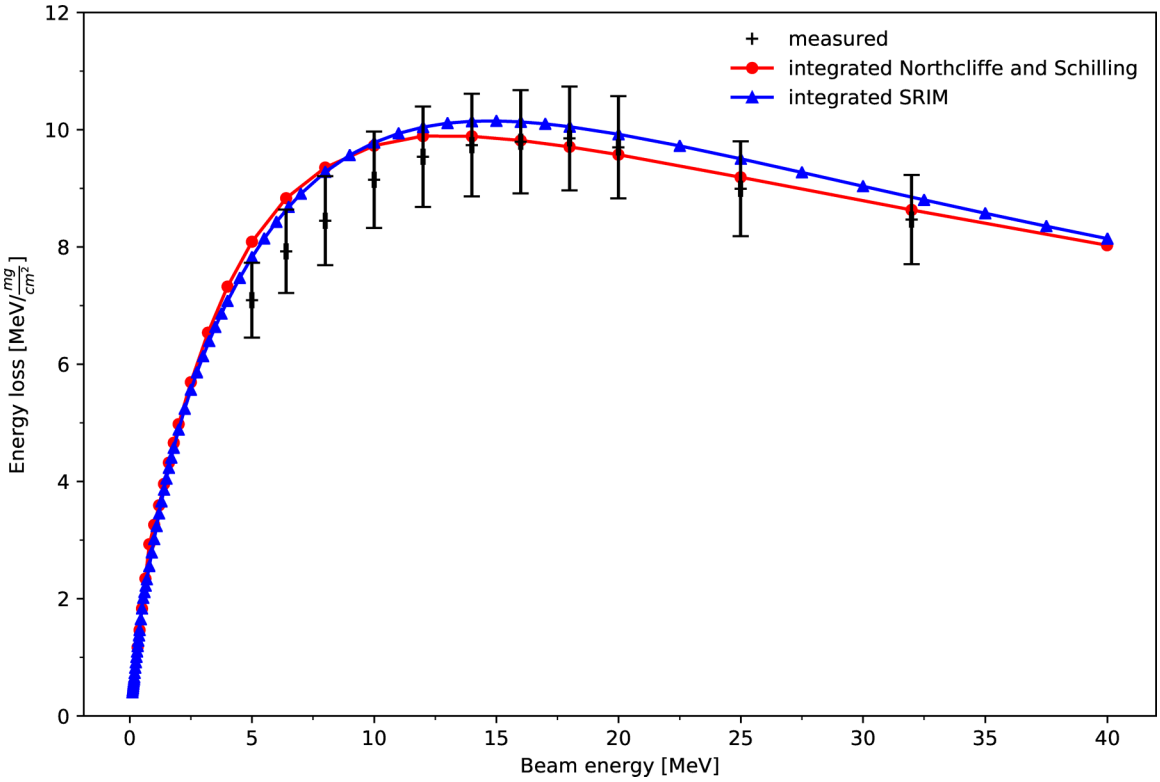

FIG. 1. Comparison of the interpolated stopping power of ^{20}Ne ions in Mg with the tabulated values of Northcliffe and Schilling [49] and SRIM [50]. These values were integrated over the foil thickness.

a direct feeding transition [gates from above (GFA)] were set on shifted fractions of the line shapes of the feeders and the approach from Ref. [57] was used. For the 2_1^+ and 4_1^+ levels in ^{22}Ne, γ-γ coincidences were again used, but the analysis was performed in the framework of the spectral difference method (SDM) [58]. The two procedures used are shortly presented below before the details of the analysis.

B. Analysis with gates from above (GFA)

As already mentioned, for every investigated line shape corresponding to a γ-ray depopulating the level of interest the slowing-down history of the ion and the time evolution of the population of the level are correlated. This mechanism relevant to γ-γ coincidence measurements is investigated in details in Ref. [57]. Referring the reader to that work, here we only note the main features of the proposed lifetime determination. Let us consider a hypothetical level scheme consisting of the levels a and b (the latter being on top). The transitions A and B depopulating these levels, correspondingly, are registered by two detectors, which may be a part of a multidetector setup (the detectors are also labeled by A and B). Different gates can be set at different locations on the shifted portion of transition B. The line shape of the transition A generated in this way has to be analyzed. This line shape is obtained by folding the spectrum of the shifted energies E_A^{Sh} [i.e., the spectrum of the velocity projections $r(v_A)$] with the detector response function $\Phi(E_A, E_A^{Sh})$. Since the gate is set on a folded spectrum, different energies E_B^{Sh}, respectively, different projections v_B, contribute to the generation of the gated spectrum. with probability to contribute $W_B(v_B)$ (for more details see Ref. [57]). Under these conditions, the spectrum of the velocity projections $r(v_A)$ for a particular slowing-down (velocity) history is given by

$$r(v_A) = b_{af}\int_0^{\infty} dt_a \int_0^{t_a} dt_b W_B\left(v_B^{\kappa}(t_b)\right)\delta\left(v_A, v_A^{\kappa}(t_a)\right)\lambda_a\lambda_b n_b \times (t_b)e^{-\lambda_a(t_a-t_b)}. \quad (1)$$

In Eq. (1), κ labels the velocity history, b_{af} is the branching ratio of the transition A ($a \rightarrow f$), i.e., from state a to the final state f while λ_a and λ_b are the decay constants of the two levels a and b, respectively. The δ function serves to increment the content of the point in the velocity spectrum with a coordinate v_A, which corresponds to the projection of the ion velocity at the emission time t_a of the transition A. The two-dimensional time plane (t_a, t_b) can be divided into three regions depending on the motion status of the excited nucleus at the moments of emission of the transitions A and B: (i) Both emissions occur during the slowing down (SS,SS); (ii) Transition B occurs in slowing down (SS), A occurs at rest (U), i.e., (SS,U); (iii) Both transitions occur at rest (U,U). By setting a gate only on the shifted component of B, the (U,U) contribution is removed. In Ref. [57] it was shown that the lifetime τ_a of the level a can be determined via the following formula

$$\tau_a = \{B_{SS}, A_U\}/(d\{B_{SS}, A_{SS}\}/dt_s), \quad (2)$$

where the quantities in brackets are coincident events and t_s is the time when the nucleus comes to rest. In practice, the area

TABLE I. Lifetimes of the 2_1^+ level in ^{20}Ne as derived in the present work with different gates set at the forward and backward rings according to the procedure [57]. See also text.

Beam energy [MeV]	Gate at 45° 2641–2675 keV	Gate at 45° 2645–2684 keV	Gate at 142.3° 2527–2574 keV	Gate at 142.3° 2535–2582 keV	$\langle\tau\rangle$
30	1.068 (52 ps	1.128 (55) ps	1.255 (56) ps	1.070 (47) ps	1.089 (34) ps
33	1.031 (20) ps	1.173 (22) ps	1.285 (22) ps	1.095 (19) ps	1.100 (79) ps
36	1.035 (31) ps	1.056 (27) ps	1.216 (28) ps	1.126 (27) ps	1.042 (78) ps

of $\{SS, U\}$ component can be fitted with the response function of the detector (normally a Gaussian) while the $\{SS, SS\}$ component can be fitted using the corresponding term in Eq. (1). More details about the latter point can be found in Ref. [57]. Here we only mention that the procedure consists of fitting both the line shape and the decay function $\lambda_a n_a(t)$ using second-order polynomials smoothly interconnected at a varying set of borders on the time scale. For every new set of borders, a summation over all MC histories of the simulation is performed to generate the quantities necessary for the reproduction of the spectrum and calculation of the derivative in the denominator of Eq. (2). An initial guess for the value of τ_a enters as an additional parameter in the fitting procedure. However, this value must be the same as the value deduced from the equation for the derivation of the lifetime [Eq. (2)]. Hence the internal consistency of the procedure is not hindered by the necessity to involve a guessed value for τ_a as a parameter. With the gate on a directly feeding transition, this method is free from the side-feeding problems which makes the derivation of lifetimes less reliable in singles measurements.

C. Results for ^{20}Ne

Because of the very intense γ-ray line at 1636 keV originating from ^{23}Na in the np-reaction channel and present in the gated spectra at the forward rings, line shapes were analyzed only at the backward rings obtained with gates on the shifted component of the 2083 keV transition, which directly feeds the 2_1^+ level. These gates were set at both rings 1 (forward with respect to the beam direction) and 2 (backward). In both cases, two slightly different gates were used with a partial overlap between them. The results obtained for the different incident beam energies are listed in Table I and illustrated for some cases in Fig. 2. Here we mention that the data taken at the beam energy of 38 MeV were not analyzed since it

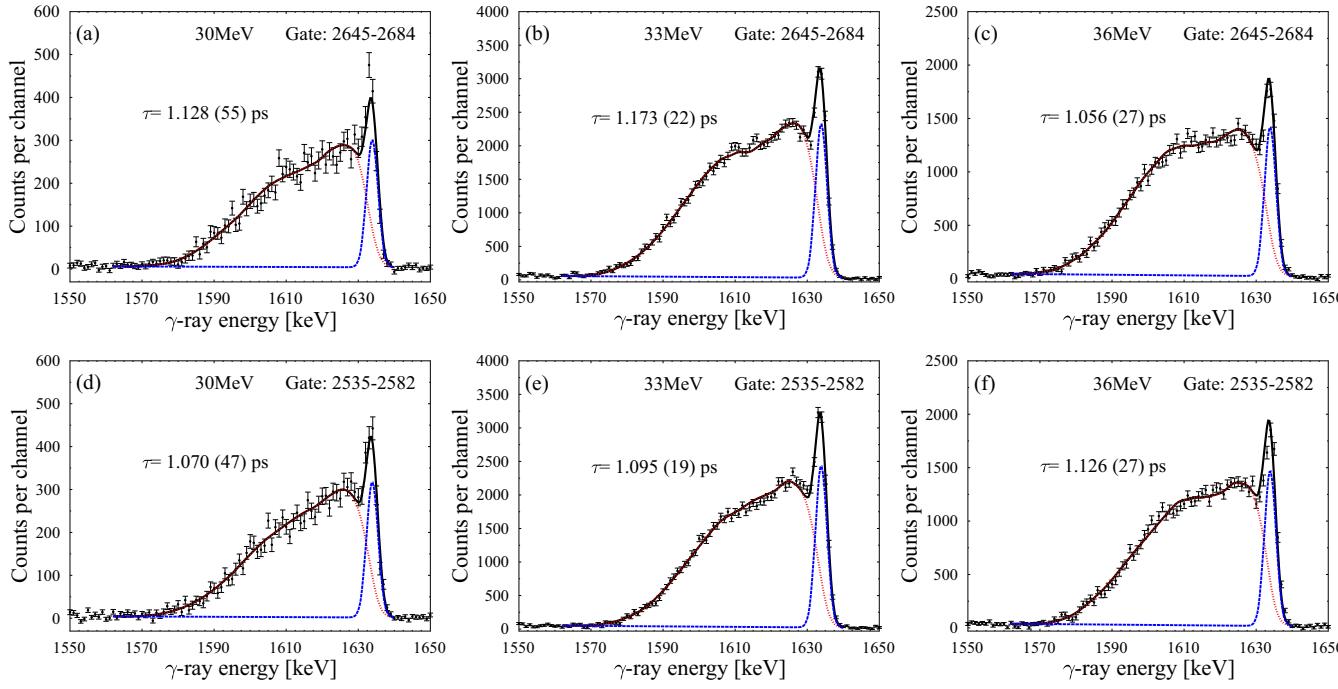

FIG. 2. Line-shape analysis and determination of the lifetime of the 2_1^+ level in ^{20}Ne within the GFA procedure with different gates set on the shifted components of the feeding transition of 2614 keV from the 4_1^+ level and at different beam energies. The gate in (a)–(c) is set at the forward ring of 45° while in (d)–(f) the gate is set at the backward ring of 142.3°. The decomposition of the full line shape of the gated transition into shifted and unshifted components is shown and the derived lifetime for each case are indicated. The width of the energy channel is 1 keV. Note the smooth evolution of the line shapes with increasing beam energy characterized by a net increase of the plateau fraction. See also text.

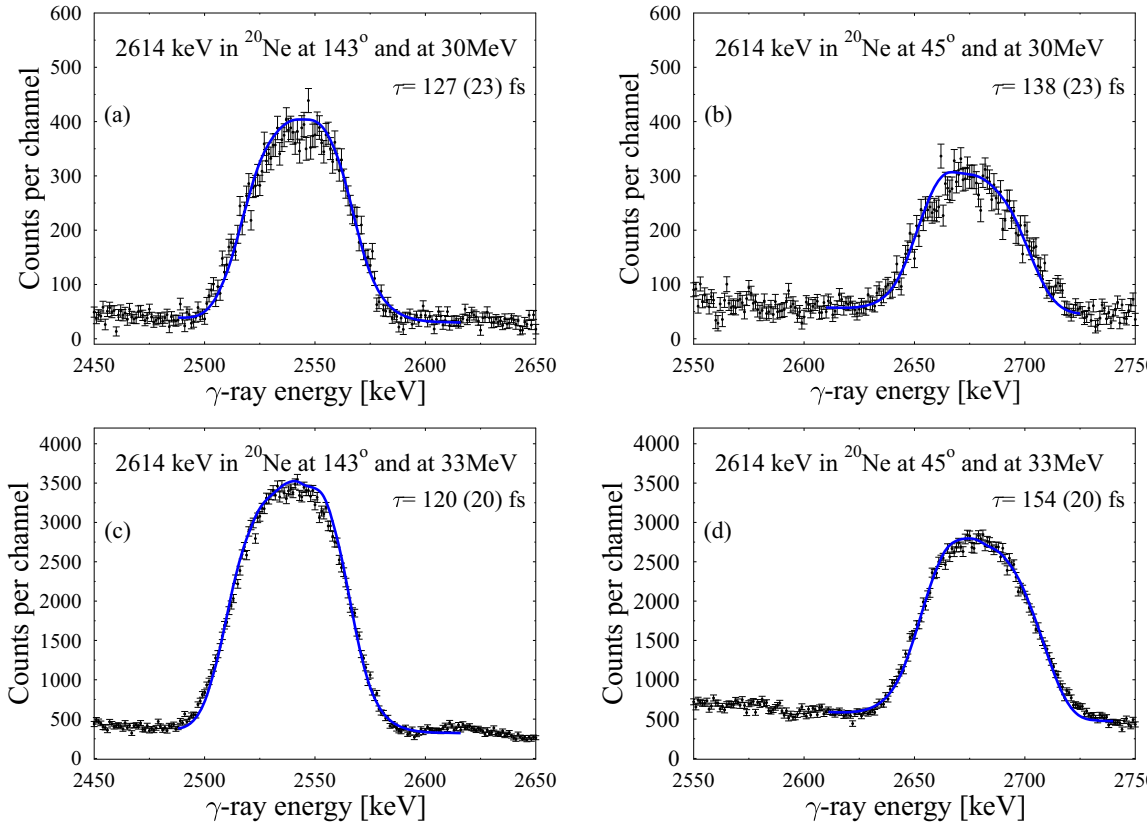

FIG. 3. Description of the line shape of the 2614 keV transition using a one-parameter fit of the 4_1^+ level lifetime and a decay function representing a single exponential function. In the top panels (a), (b), the fits of the line shapes observed at the angles of 143° and 45° at the beam energy of 30 MeV are shown. The corresponding data at 33 MeV are shown in the bottom panels (c), (d). The effective lifetimes derived by the analysis of the χ^2 curve are indicated. See also text.

turned out that at this energy some fraction of the recoils leaves the target-stopper compound, which makes an eventual analysis much more difficult and unreliable. As can be seen, the lifetimes in the fourth column (gate 2527–2574 keV) systematically deviate to larger values than the others. Most probably this is due to the presence of a contaminant γ ray in that gate. Therefore they were not taken into account in the averaging to obtain the final value of $\tau = 1.087(48)$ ps where the uncertainty is purely statistical. Concerning the uncertainty related to the incomplete knowledge of the stopping powers, we note that in Ref. [59] it was shown that the approach of Ref. [57] is robust against scaling variations of the stopping powers. Nevertheless, we estimate the uncertainty to be 3% taking into account conservatively the experimental uncertainties of our stopping power experiment, which do not exceed 10% as usually. Thus, by adding in quadrature the latter uncertainty of 3% we obtain the final result:

$$\tau(2_1^+ \text{ in } ^{20}\text{Ne}) = 1.087(60)\,\text{ps}.$$

This result is in an extremely good agreement with the averaged value from the literature [33] of $\tau = 1.053(58)$ ps. From our new lifetime result a value for the reduced transition strength of $B(E2; 2_1^+ \rightarrow 0_1^+) = 0.00645(61)e^2b^2 = 20.0\ (1.9)$ W.u. is determined. Thus, the strong collectivity of the $2_1^+ \rightarrow 0_1^+$ transition in ^{20}Ne is again confirmed, with more advanced measuring at analysis. The situation for the 4_1^+ level is different. No feeding transitions were observed by us over the energy range of γ rays detectable by our setup (up to 4.5–5.0 MeV). Also, at the lower beam energies used such hypothetical states would be in principle unbound. Therefore we performed a line-shape analysis using a single-exponential decay function with the only parameter being the lifetime of the 4_1^+ state but we shall call in the following this parameter effective lifetime τ_{eff} to stress that it may contain a feeding-delayed contribution. The results are presented in Table II while the analysis is illustrated in Fig. 3. One should note that the mean lifetimes derived from the data taken at 30 MeV and 33 MeV in practice coincide, which seem to give some support to the direct population of the level considered in the reaction used. Differently from the case of 2_1^+ state, here we estimate, although somewhat conservatively, the uncertainty in the lifetime related to the incomplete knowledge of the stopping powers to 6% (i.e., twice more). Adding in quadrature this uncertainty leads to the final result for the 4_1^+ level averaged from the 30 MeV and 33 MeV:

$$\tau_{\text{eff}}(4_1^+ \text{ in } ^{20}\text{Ne}) = 136(20)\,\text{fs}.$$

This points to a significantly longer effective lifetime than the literature value for the lifetime of 92 (9) fs [33]. However, since we cannot exclude some feeding equally present both in the 30 and 33 MeV data, we give the limit:

$$\tau(4_1^+ \text{ in} ^{20}\text{Ne}) \leqslant 156\,\text{fs}.$$

TABLE II. Effective lifetimes of the 4_1^+ level in ^{20}Ne as derived in the present work with different gates set at the forward and backward on the full line shape of the $2_1^+ \rightarrow 0_1^+$ transition and single-exponential fit. The average effective lifetime $\langle\tau_{\rm eff}\rangle$ over the four cases is shown in the last column. See also text.

Beam energy [MeV]	Gate at 45° 45°	Gate at 45° 143°	Gate at 142.3° 45°	Gate at 142.3° 143°	$\langle\tau_{\rm eff}\rangle$
30	138 (23) fs	124 (25) fs	160 (25) fs	127 (23) fs	137 (16) fs
33	154 (20) fs	113 (27) fs	155 (20) fs	120 (20) fs	136 (22) fs

Correspondingly, one obtains for the transition strength $B(E2; 4{+}_1 \rightarrow 2_1^+) \geqslant 0.00429 e^2b^2 \geqslant 13.3$ W.u.

D. Analysis within the SDM

The attempts to analyze the data for ^{22}Ne with the same approach as in the case of ^{20}Ne turned out to be unsuccessful due to the long lifetime of the first 2^+ level (in any case more than 2 ps). Therefore, the data, i.e., the line shapes, do not possess enough sensitivity to the decay function $\lambda n(t)$ at times larger than the stopping time of the ion. Thus, we applied a relatively new method [58], which was later called the spectral difference method (SDM). In SDM, similarly to the differential decay curve method (DDCM) (for derivation for Doppler-shifted line shapes see Ref. [60]), the decay function of the transition of interest is first determined. The feeding of the level is included via the spectral difference of two successive Doppler shifted decays (i.e., the difference of the two corresponding γ-ray line shapes). This new approach has been tested for the case of the Blaugrund approximation in Ref. [63] and for the Monte Carlo approach in Ref. [58]. In general, the energies E_B and E_A of a feeding (B) and a deexciting transition (A) of the level of interest are different. However, the right part of the Doppler formula $E_{\gamma,sh}(t) = E_{\gamma,0}[1 + \frac{v(t)}{c}\cos(\theta(t))]$ is the same for both transitions. Therefore, one transition can be transferred (shifted) into the energy range of the second one by the transformation:

$$E'_{\gamma,sh}(B) = \frac{E_{\gamma,0}(A)}{E_{\gamma,0}(B)} E_{sh}(B). \tag{3}$$

After transformation of the line shapes of A and B into the same energy range, the difference D of both spectra in terms of velocity projections v_θ can be calculated according to:

$$\begin{aligned} D(v_\theta) &= S_B(v_\theta) - S_A(v_\theta) \\ &= \int_0^\infty (\lambda_B n_B(t) - \lambda_A n_A(t)) P_\theta(t, v_\theta) dt, \end{aligned} \tag{4}$$

where S_B and S_A are the line shapes in terms of velocity projections given by $S_i(\tau, v_\theta) = \lambda_i \int_0^\infty P_\theta(t, v_\theta) n_i(t) dt$, $n_i(t)$ being the number of nuclei in state i at time t. Solving the above integral with partial integration and using the Bateman equations leads to

$$D(v_\theta) = \int_0^\infty \frac{\partial P_\theta(t, v_\theta)}{\partial t} n_A(t) dt, \tag{5}$$

where $\partial P_\theta(t, v_\theta)\partial t$ is the numerical derivative of the stopping matrix. The above equations hold also in terms of γ-ray energy spectra obtained after folding with the detector response function. By using the spectral difference of both transitions, one can solve the integral Eq. (5) for $n_A^D(t)$, where D indicates the origin of this quantity from the fit of the difference. On the other hand, the quantity $\lambda_A n_A^S(t)$ represents the decay function of transition A, which can be determined according to the DDCM procedure described in Ref. [60] and applied in Ref. [64], where S denotes its origin from a fit of the spectrum of the deexciting transition. It follows that, dividing $n_A^D(t)$ by $\lambda_A n_A^S(t)$ should yield a constant value for the level lifetime as a function of t, i.e.,

$$\tau(t) = \frac{n_A^D(t)}{\lambda_A n_A^S(t)} = \frac{1}{\lambda_A}. \tag{6}$$

Since a level has one distinguished lifetime, the result of Eq. (6) should be a constant function in t, which represents the so-called τ curve. However, it is clear that the values of the decay functions are small for very low and very large values of t and therefore the ratio calculated in Eq. (6) is not stable at these conditions. Thus, the determination of the lifetime $\tau(t)$ via a linear fit is concentrated solely in a region of sensitivity. This region should be taken as about half of the maximum of the decay function on both sides of the maximum. The final level lifetime is determined as a weighted average of all values $\tau(t)$ in the region of sensitivity [60]. For SDM, by setting a coincidence gate on the feeding transition, no unknown side feeding has to be taken into account. Consequently, the determined lifetime is the real lifetime of the level of interest.

E. Results for ^{22}Ne

For applying the SDM [58], wide gates on the whole line shapes of the feeding transition of 2083 keV and on the depopulating transition of 1275 keV were set at the forward and backward rings in four γ-γ coincidence matrices. Thus, four gated spectra were obtained for each of the transitions of interest. After careful subtraction of the background, the corresponding pairs of line shapes were analyzed according to the procedure outlined in the previous section. The same operations were performed for the case of the 4_1^+ level where also a wide gate on the populating transition of 2954 keV from the 6_1^+ level was used. The lifetime results are presented in Table III. The procedure is illustrated for the symmetric γ-γ coincidence matrices in Figs. 4 and 5. The statistical averaging of the results in Table III leads to the mean value of $\tau_{\rm stat}(2_1^+) = 2930$ (60) fs. Again estimating the uncertainty in the lifetime related to the incomplete knowledge of the stopping powers to 6%, adding in quadrature this uncertainty leads to the final result:

$$\tau(2_1^+ \text{ level in } {}^{22}\text{Ne}) = 2930(190)\,\text{fs}.$$

TABLE III. Lifetimes of the 2_1^+ and 4_1^+ levels in ^{22}Ne as derived in the present work with the SDM when using different two-ring combinations, which are indicated in the first row of the table. The wide gate is set at the second of the indicated rings while the generated line shape to analyze is observed at the first ring. See also text.

Level	45°–45°	45°–142.3°	142.3°–142.3°	142.3°–45°
2_1^+	2921 (45) fs	2851 (33) fs	2990 (40) fs	2941 (47) fs
4_1^+	216 (30) fs	213 (5) fs	202 (17) fs	202 (17) fs

This value is quite different from the averaged value from the literature [66] of $\tau = 5134\ (72)$ fs being smaller by about 43%. Correspondingly, the absolute reduced transition strength for the 2_1^+ level is $B(E2; 2_1^+ \rightarrow 0_1^+) = 0.00828\ (54) e^2b^2 = 22.6\ (1.5)$ W.u. Therefore, the quadrupole collectivity is as strong as that in ^{20}Ne [where $B(E2; 2_1^+ \rightarrow 0_1^+) = 20.0\ (1.9)$ W.u.]. It should be mentioned that in the case of the 4_1^+ level it was not possible again to use the GFA method with a partial gated on the shifted component of the direct feeder of 2954 keV since there is (nearly) no hint for an unshifted peak in the line shape of the 2083 keV

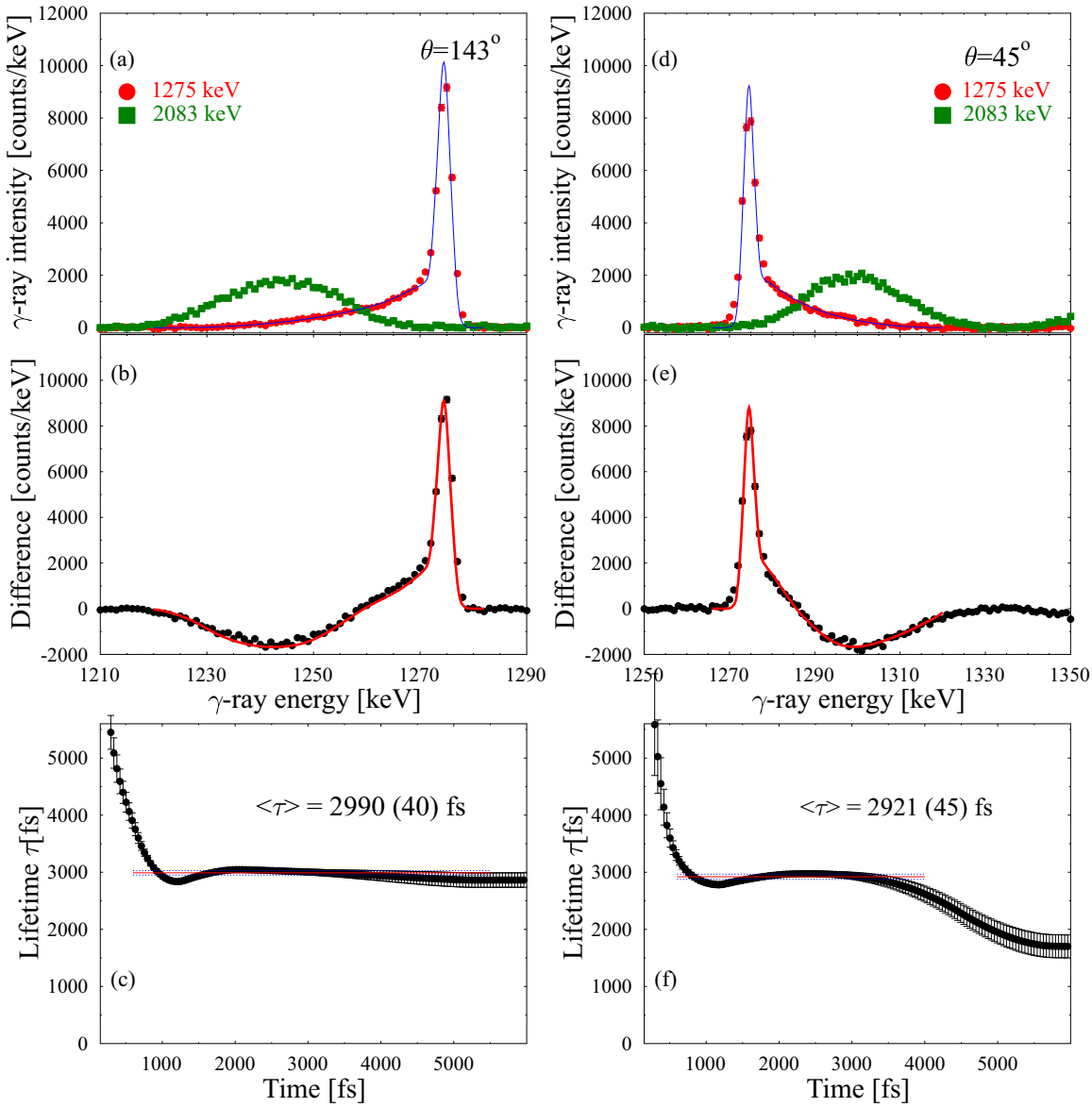

FIG. 4. Analysis within the SDM of the pair of subsequent transitions $4_1^+ \rightarrow 2_1^+ \rightarrow 0_1^+$ in ^{22}Ne at the angles indicated. In the top panels (a), (d), the line shapes are displayed after background subtraction and conversion of the line shape of the 2083 keV transition on the range of the 1275 keV one. The fit of the line shape of the latter transition is also shown. In the middle panels (b), (e), the difference of the two line shapes from the top panels is shown with its fit. The lifetime derivation using the τ curve is illustrated in the bottom panels (c), (f). See also text.

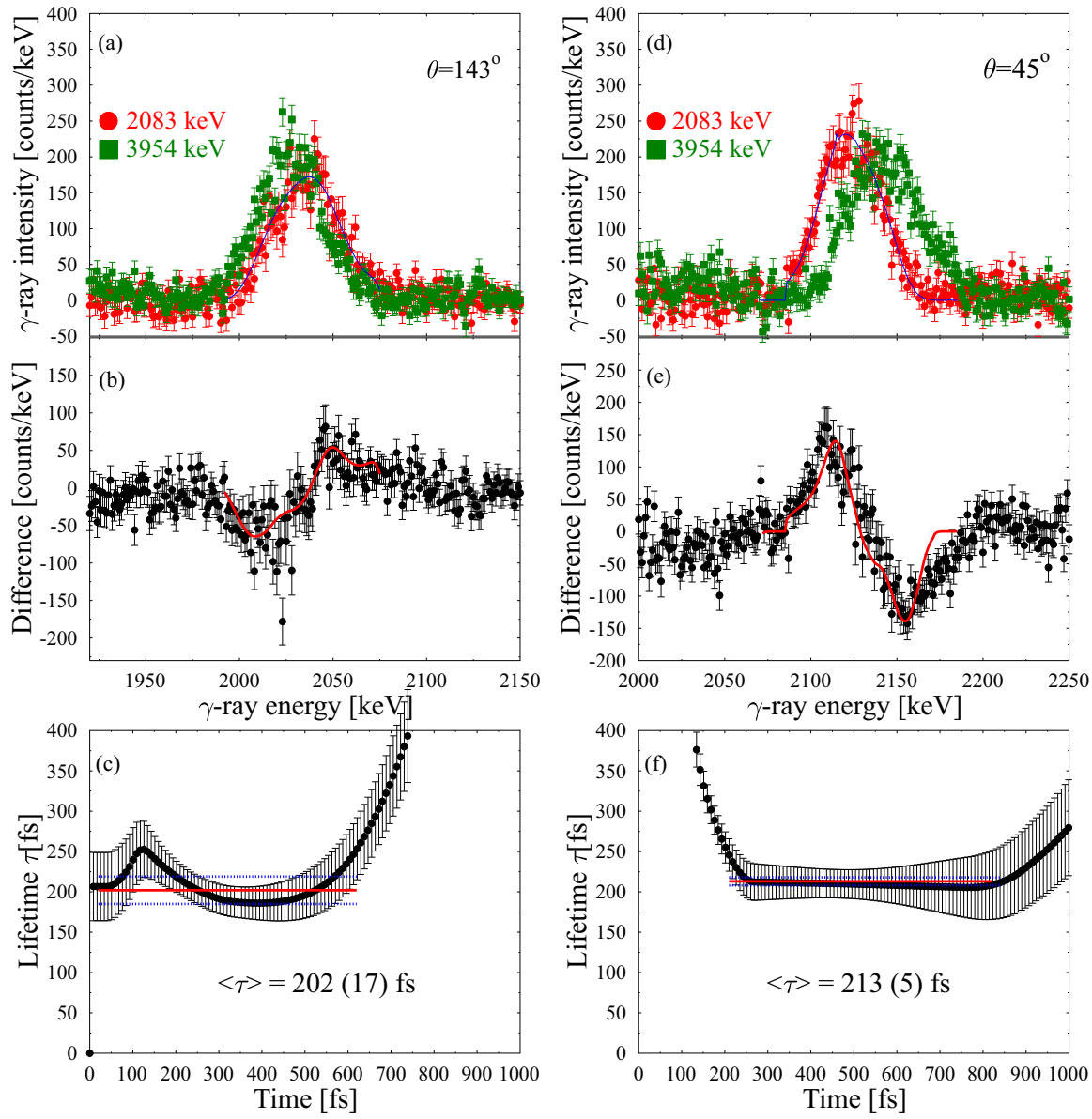

FIG. 5. The same as in Fig. 4 but for the pair of subsequent transitions $6_1^+ \rightarrow 4_1^+ \rightarrow 2_1^+$ at the angles indicated. Note the smaller Doppler shift at the backward angle, which makes the analysis more difficult. A small contamination at the far end of the shifted 2954 keV transition at 45° leads to some drop in the spectral difference which of course cannot be reproduced by a fit (middle panel on the right). See also text.

transition, which makes impossible or very insecure to use Eq. (2) for the lifetime derivation. Thus, we applied again the SDM as for the 2_1^+ level. Applying the same approach for taking into account the uncertainties related to the stopping powers as for the 2_1^+ level, we obtain for the 4_1^+ level the final result:

$$\tau(4_1^+ \text{ level in } {}^{22}\text{Ne}) = 212(26)\,\text{fs}.$$

This value is again shorter than the averaged result from the literature of $\tau = 325$ (6) fs [66]. The corresponding reduced transition strength is $B(E2; 4_1^+ \rightarrow 2_1^+) = 0.00983$ (121) $e^2b^2 = 26.8$ (3.3) W.u.) indicating a possible increase of collectivity at the 4_1^+ level.

The shorter lifetimes presently derived for both 2_1^+ and 4_1^+ states with about 40% decrease tend to indicate that the stopping powers used in previous DSAM analyses were not correct. However, most of the previous measurements employed the plunger (RDDS) method where stopping powers play not at all or a rather marginal role. For these plunger cases other explanations for the discrepancy have to be looked for. The same holds for the lifetime determinations in ^{22}Ne using Coulomb excitation [61] and inelastic electron scattering [62] and all this will be shortly discussed below. Since such developments with respect to lifetime values may seem a bit unexpected, we have performed an additional analysis using the same description of the slowing-down process as above, but modeling the decay function of the 2_1^+ state in its original (fundamental) form. Namely, as a solution of the Bateman equations, it is represented by a superposition of exponential functions with decay constants and weights fixed

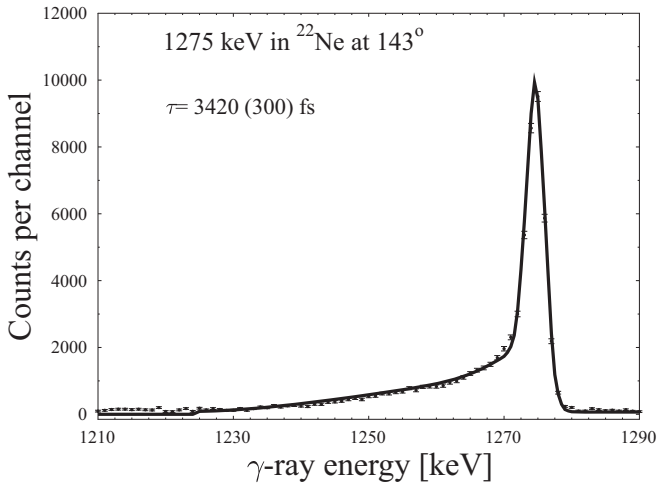

FIG. 6. Description of the line shape of the 1275 keV transition using a one-parameter fit of the 2_1^+ level lifetime and a decay function representing a superposition of exponential functions with the participation also of the 4_1^+ level (lifetime from the present work) and of the 6_1^+ level (lifetime form [66]). See also text.

by the properties of every particular cascade of excited nuclear levels. In the present case, we employed a three-level cascade including the 2_1^+, 4_1^+, and 6_1^+ levels. The newly determined lifetime of the 4_1^+ level was used and for the 6_1^+ level the value of $\tau = 71$ fs was taken from the literature [66]. Careful checks showed that the latter value is consistent with a line shape analysis based on our data. The γ-ray line shape of the 1275 keV $2_1^+ \rightarrow 0_1^+$ transition was generated by a wide gate set on the line shape of the 2083 keV $4_1^+ \rightarrow 2_1^+$ transition in the 142.3°–142.3° γ-γ coincidence matrix. After adjusting the total area of the line shape within the fitting procedure, the lifetime of the 2_1^+ level was varied till the best χ^2 value of the fit was obtained. This final result is shown in Fig. 6. Obviously the result for $\tau = 3420$ (300) fs is quite consistent with what was obtained with the SDM, especially when taking into account that with the approach of representing the decay function as a superposition of exponential functions the gating on the $4_1^+ \rightarrow 2_1^+$ transition may lead to including in the cascade levels above the 4_1^+ one (and above the 6_1^+ too, of course). Therefore we think that the correction of the old literature τ value by about 43% is really taking place and necessary. A systematics of the experimental results on the lifetime of the 2_1^+ level before 1984 can be found in Table I of Ref. [44]. Most of them were obtained using the RDDS (plunger) method and point to $\tau \approx 5.2$ ps. However, the methods of analysis used in these works were those employed before the establishment of the DDCM [60,65] as the most reliable tool in that field. Also, no γ-γ coincidences and gating on feeding transitions were employed (only gating on particles to purify the spectra in some cases). Therefore these previous measurements are subject to significant influence of the side-feeding problems leading when not taken properly into account to the derivation of longer lifetimes. Although Coulomb excitation (CE) is quite different and indirect technique compared to RDDS, in the work [61] dedicated to ^{22}Ne, its application has a common feature as stated by the authors—many states populated above the 2_1^+ one. This again suggests that the reason for the discrepancy with the present smaller lifetime result is due to not correctly taken into account side-feeding effect in the previous investigations. Other reasons for differences with indirect methods may exist as (partial) model dependences emphasizing electron scattering but will not be considered here. They are best described in Refs. [61,62] pointing out the difficulties in the analysis, e.g., angular distribution for the Coulomb excitation experiment including possible time dependence or model-dependent extrapolation to low momentum transfer for electron scattering.

F. Consistency check: The SDM applied to the 2_1^+ level in ^{20}Ne

In addition, it was decided to perform a consistency check of the two procedures employed in the present work by analyzing with the SDM the data for the 2_1^+ level in ^{20}Ne, apart of the GFA analysis described above. In this way, possible methodological problems could be confronted to reality and more reliable conclusions could be made on our results for ^{22}Ne, which differ so much from the literature. This investigation is illustrated in Fig. 7 for three different incident beam energies. Obviously, due to the small lifetime of the 4_1^+ level as well as the huge difference in energy of the depopulating transitions, the technical application of the SDM is more difficult in this case (^{20}Ne) compared to ^{22}Ne (we note the already mentioned and yet unsolved problem of the different detector resolutions for the two γ's). The scattering of the SDM values is significant at this level of statistics, but the average value of 0.92 (10) ps is in reasonable agreement with the result of $\tau = 1.09$ (6) ps derived with the GFA method. Simultaneously, the behavior of the systematic deviations of the lifetime derived with the SDM are easy to explain. First, the tendency to smaller lifetime values is related to the much bigger FWHM of the feeding transition with higher energy. Then, the counts in a specific channel of its spectrum should be actually a part of a quantity spread over more channels this leading to a smaller difference than in reality. Therefore, as already mentioned, since the different FWHM's are not taken precisely into account at present this leads to the effect of artificial decrease of the lifetime during its calculation. With the increase of the beam energy, i.e., of the Doppler shift and with the line shape covering more channels, the latter effects increases, indeed (compare the τ panels for 30, 33, and 36 MeV beam energy). These findings give not only a strong support to the results derived for ^{20,22}Ne presently, but also provide some validation of the use of SDM in practical cases while still showing the necessity to improve its technical implementation.

IV. DISCUSSION

We start our considerations with a discussion of systematic calculations within the shell model and configuration mixing approaches mainly in the context of the comparison between them and the experimental results for the $B(E2; 2_1^+ \rightarrow 0_1^+)$ values, including the present ones, in the chain of even-even Ne isotopes. We decided to not perform new calculations of that type since we are not optimistic about the possibility to

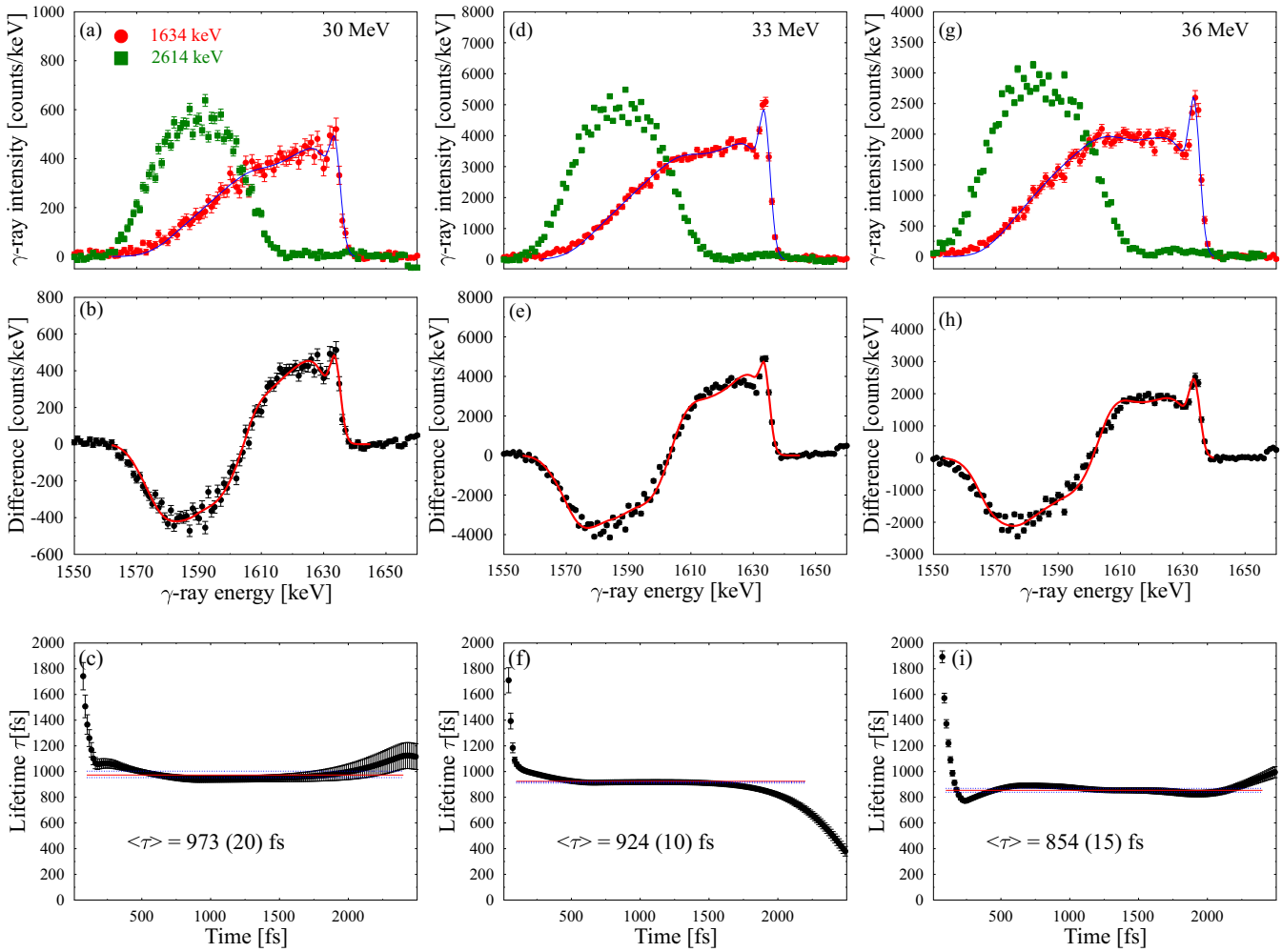

FIG. 7. Analysis of the pairs of 1634 and 2614 keV in ^{20}Ne at three different beam energies according to the SDM. The meaning of the information displayed is the same as in Fig. 4 but for the specific case presented here. See also text.

improve on the earlier calculations in the literature. After that, we compare our new transition strength data for the 2_1^+ and 4_1^+ to calculations aiming to reproduce such quantities as well the level schemes of ^{20,22}Ne. Finally, we consider the possibility to describe the $B(E2)$ data in the framework of cluster models before going to the conclusions.

A. Shell-model calculations

1. Systematics of the $B(E2; 2_1^+ \rightarrow 0_1^+)$ values in the Ne isotopes

A longstanding problem in nuclear theory is the missing quadrupole collectivity necessary to reproduce the $B(E2; 2_1^+ \rightarrow 0_1^+)$ reduced transition strengths in the mass region $A = 20$–30, and in particular, in ^{20,22}Ne (see for discussion, e.g., Ref. [8]). In Fig. 8 we present the available experimental data compared to quite recent systematic theoretical calculations. The first ones, indicated by the label MpMhCM are the multiparticle-multihole configuration mixing calculations from Ref. [8], which have been already mentioned. These results are taken from Fig. 6 in that work and have two versions. The first version shows the worse agreement with the data, especially for ^{20,22}Ne where the increase of the $B(E2)$ values compared to the heavier isotopes is marginal and not sufficient. The authors of Ref. [8] allowing some scaling of the $B(E2)$ values based on considerations similar to taking into account effective charges arrive to the second data set labeled by MpMhCM*2.83 in Fig. 8. This scaled data set achieves an improvement of the description for $^{24-28}$Ne but fails to do the same for ^{20,22}Ne. According to Ref. [8] and as already mentioned, the MpMhCM results indicate missing collectivity in the standard approaches aiming to reproduce the quadrupole properties in the mass region $A = 20$–30. The calculation labeled EKK [10] represents an application of the so-called Kuo-Krenciglowa theory of the effective nucleon-nucleon interaction to shell-model studies. One of the success of this approach is the first shell-model description of the island of inversion without fitting interactions. The EKK calculation is again successful for the heavier isotopes but it fails again to reproduce the $B(E2)$ values in ^{20,22}Ne. The calculation from Ref. [15] represents an investigation of the Ne isotopes within a framework based on energy functionals and is indicated by the label DD-PC1 in Fig. 8 following the notations of the authors. The authors first build deformation energy surfaces with self-consistent relativistic

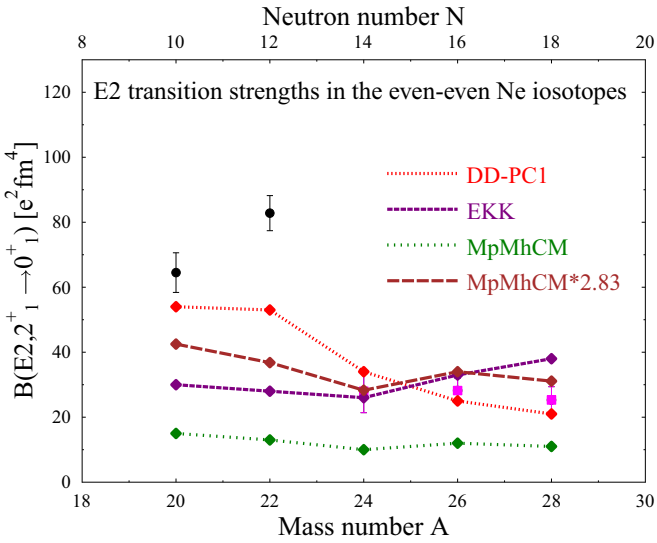

FIG. 8. Experimental data on $B(E2)$ transition strengths from the present work (circles) and from the literature (squares) compared to different calculations as function of the mass number A. See also text.

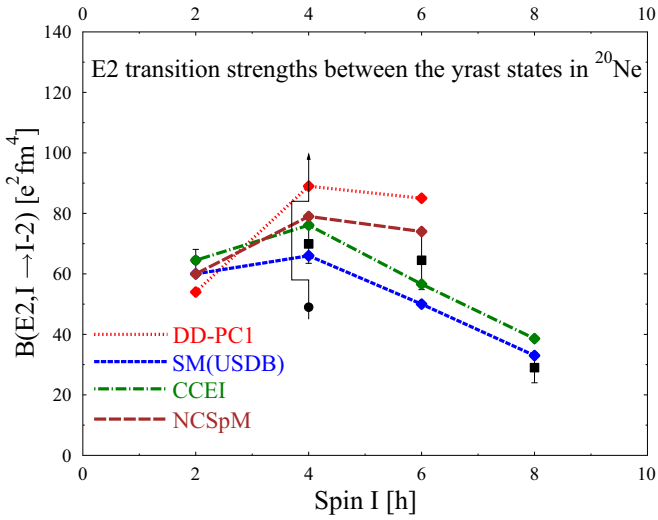

FIG. 9. Experimental data on $B(E2)$ transition strengths in ^{20}Ne from the present work (circles) and from the literature (squares) compared to different calculations as function of the spin I. See also text.

Hartree-Bogoliubov calculations and then construct collective symmetry-conserving states using projection techniques and the generator coordinate method. An interesting aspect is the inclusion of cluster-state configurations. This calculation gives the best description of the data but still cannot reproduce the enhancement in ^{22}Ne. Nevertheless, because the $B(E2)$ data for ^{20,22}Ne are not so faraway from each other, one may consider that this approach is successful and it might be a question of fine adjustments to obtain a completely consistent picture.

2. *Spin dependence of the E2 transition strengths between the yrast states in* ^{20,22}Ne

In this section, we consider theoretical calculations aimed to the concrete detailed description of the level schemes of ^{20,22}Ne, also at higher energies and spins that the 2_1^+ level. While in the systematics of the $B(E2; 2_1^+ \rightarrow 0_1^+)$ values in the Ne isotopic chain the already mentioned calculation DD-PC1 [15] was quite successful, it seems to overestimate the transition strengths at higher spin between the yrast states. A more successful calculation is that labeled by NCSpM in the nomenclature of the authors [11]. It is based on the no-core symplectic shell model (origin of the abbreviation) for symmetry-preserving interactions (for more details see Ref. [11]). The essential point is that no parameter adjustments are applied although the model is not fully *ab initio*. Still the data for the $I^\pi = 8^+$ level seems to be difficult to be reproduced by an extrapolation of the NCSpM results. Two calculations give a nearly similar and satisfactory description of the data. The first one is that labeled by SM(USDB) in Fig. 9 and the data is taken from Ref. [12]. In this work the nucleon-pair approximation is studied by employing both schematic and effective interactions, and in the latter case a good description of the properties of ^{20}Ne is obtained. It should be mentioned that the corresponding data on Fig. 9 is taken from column 3 of Table IV in Ref. [12] where other theoretical values for different interactions and approximations are also given. This particular set of data gives also a very good description of level energies compared to experimental ones. It should be mentioned that these theoretical values are normalized to the $B(E2; 2_1^+ \rightarrow 0_1^+)$ transition strength and therefore we used our experimental result to scale these quantities to the Y scale of Fig. 9. The calculation labeled CCEI [14] agrees the best with the experimental data, also without normalization or effective charges. The authors of Ref. [14] perform an extension of the *ab initio* coupled-cluster effective interaction method to open-shell nuclei with respect to both protons and neutrons. They reproduce successfully both energy spectra and transition strengths in ^{20}Ne. It should be mentioned that their method is much closer to the fundamental from first principles approach than any of the other calculations considered above, which seems encouraging for nuclear theory.

The calculations considered so far in this section and which also have predictions for ^{22}Ne are less successful in that case. This can be seen in Fig. 10 where the theoretical values from the calculations DD-PC1 [15] and NCSpM [11] are also presented. Although the overall scale (magnitude) of the data is reached, the fine details of the evolution with spin are not reproduced. It would be interesting to test in the future if a CCEI [14] calculation will have the same success in ^{22}Ne as in ^{20}Ne.

B. Cluster-model approach

In this section, we will first consider the $B(E2; 2_1^+ \rightarrow 0_1^+)$ values in ^{20,22}Ne in the framework of a generalization of the simple model used by us in Ref. [22] where to explain the low-lying quadrupole properties of the nucleus ^{32}S a large scale clusterization was invoked. Namely, this clusterization involves two doubly magic ^{16}O nuclei. Then, because of the axial and R_π symmetries it was possible to use the standard

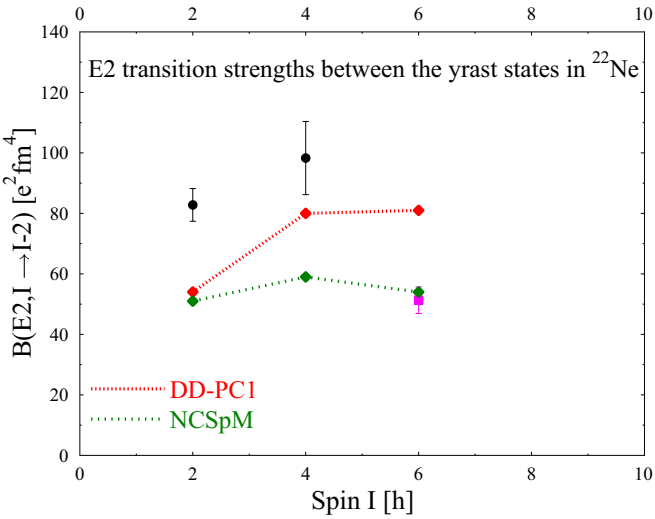

FIG. 10. The same as in Fig. 9 but for ^{22}Ne. See also text.

rotational formula for the reduced $B(E2)$ transition strength in a $K = 0$ band

$$B(E2; 2 \to 0) = \frac{5}{16\pi}\langle 2020|00\rangle^2 Q_0^2. \tag{7}$$

It is possible to show, however, that this formula is valid even in the absence of R_π symmetry for axial rotors [67]. In the Appendix of the present work, we show the expressions for the volume and quadrupole integrals and calculate the intrinsic quadrupole moment of a system consisting of two overlapping spheres with different radii. Such system is schematically presented in Fig. 11. The assumption is that the low-lying quadrupole states can be considered as a superposition of cluster states (*cl*) and (nearly) spherical states (*sph*)

$$|\Psi\rangle = A_{cl}|\Phi\rangle + A_{\rm sph}|\Theta\rangle. \tag{8}$$

However, an inspection of the level schemes of ^{20,22}Ne [33,66] suggests, because the possible partners of the 0_1^+ and 2_1^+ within such mixing lie quite high in energy, that a two- (or three-)band mixing calculation is difficult to be performed. We mention here that similar mixing with core excitations was employed in Ref. [68] for the interpretation of ^{44}Ti lifetime data in order to enhance the total transition strength in addition to the one predicted by a cluster model calculation for that nucleus. Therefore we follow a more phenomenological approach, and concentrate on the $B(E2)$'s themselves while trying to learn more about the possible range of intrinsic quadrupole moments and mixing amplitudes. For this purpose, we assume also that the composition of the wave functions of the 2_1^+ and 0_1^+ states is similar with respect to the weights of the unperturbed states. Then, the experimental $E2$ reduced matrix element is given by

$$\langle 0_1^+||E2||2_1^+\rangle_{\rm exp} = A_{cl}^2\sqrt{\frac{25}{16\pi}}\langle 2020|00\rangle Q_0 + \left(1 - A_{cl}^2\right)\langle 0_1^+||E2||2_1^+\rangle_{\rm sph}, \tag{9}$$

where the usual assumption for neglectable contribution of transitions between the cluster and spherical wave-function

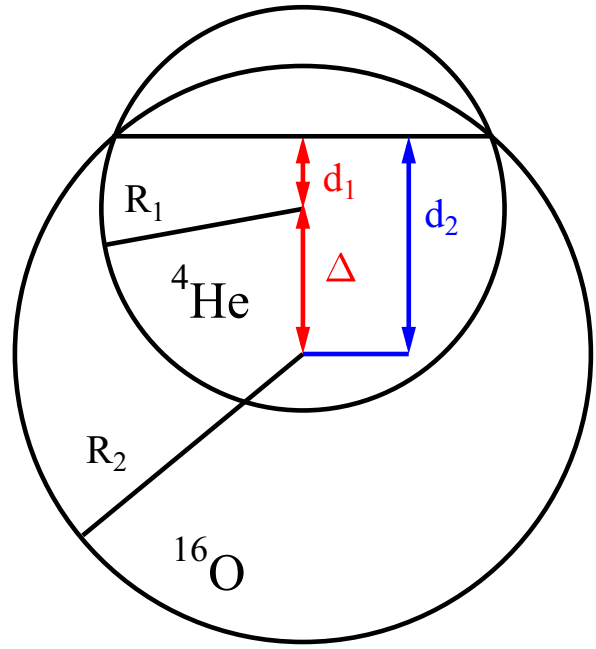

FIG. 11. Schematic representation of the system of two overlapping spheres with different radii R_1 and R_2. The first one of them is associated with ^{4}He while the second one is associated with ^{16}O. The distances to the intersection plane d_1 and d_2 are also indicated. See also text.

components is made. Here, we involve in the considerations also the data for the three heavier isotopes ^{24,26,28}Ne. To make the above estimate quantitative, the theoretical reduced $E2$ matrix elements from Ref. [8] were used, which can be derived from Fig. 6 in that work. The experimental matrix elements are from the present work or taken from Refs. [69–71] for the heavier isotopes. Equation (9) can be solved with respect to Q_0 as a function of A_{cl}^2. The results are shown in Fig. 12. In Ref. [23], detailed and much more advanced theoretical calculations than the simple model presented here were performed to reproduce the level scheme and electromagnetic transition strengths in ^{20}Ne while considering the latter nucleus as a system of $\alpha \otimes {}^{16}$O. The result [23] for the $B(E2; 2_1^+ \to 0_1^+)$ transition strength is 53 e^2fm^4, which implies, in terms of the present considerations, a value of $Q_0 = 51.6\ efm^2$. It should be mentioned that we dispose with such independent theoretical value in terms of α clustering only for ^{20}Ne. A straight horizontal line is drawn in Fig. 12 over all the range of squared amplitudes of the admixed cluster states. Obviously, the calculations in Ref. [23] are consistent with very pure ($A_{cl}^2 \geqslant 95\%$) cluster structure of the 0_1^+ and 2_1^+ levels in ^{20}Ne. Figure 12 immediately suggests the existence of similar structures in ^{22}Ne where Q_0 might be even a bit higher although the effect is within the experimental uncertainties. For the heavier isotopes, the situation is different. There, relatively small cluster-state admixtures of the order of 25%–40% and reasonable values of Q_0 are sufficient to reproduce the experimental data. In this way, the problem of the missing collectivity in the even-even Ne isotopes pointed out in Ref. [8] has one possible solution,

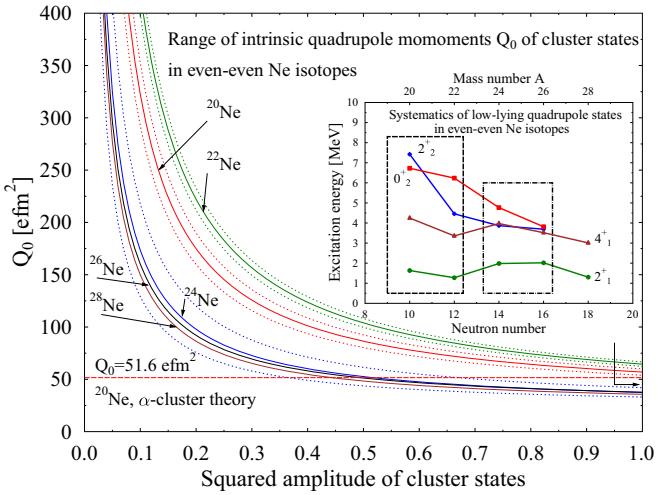

FIG. 12. Calculation of the intrinsic quadrupole moments of the cluster states in $^{20-28}$Ne after solving Eq. (9) for them and for the whole range of possible squared amplitudes. In the far-most right on the bottom the range of possible values for ^{20}Ne consistent with the results of Ref. [23] is indicated. In the insert, a systematics of the low-lying quadrupole states in $^{20-28}$Ne is presented. See also text.

which may be worth investigating with more advanced and fundamental theoretical calculations.

These findings seem to be consistent with the systematics of the lowest quadrupole states in $^{20-28}$Ne presented in the insert to Fig. 12. Obviously the level energies suggest deformed (but not identical) structures for ^{20,22}Ne and a vibrational-like character for ^{24,26}Ne as sketched by the two zones in rectangles. For ^{20,22}Ne the mean energy ratio $R(4/2) = E(4_1^+)/E(2_1^+) \approx 2.6$ while for ^{24,26}Ne$R(4/2) \approx 1.9$, which is a clear indication for a structural change in between. Some hints are also given by the Nilsson diagram for *sd* nuclei. For $N \leqslant 12$ (^{22}Ne) the neutrons are lying on orbitals favoring the prolate deformation, while at $N = 14$ the situation changes since the 5/2[202] orbital favors oblate deformation. This might be related to the indication for γ softness given in ^{24}Ne by the 4_1^+ and 2_2^+ levels forming a kind of doublet. The Nilsson diagram indicates also that ^{22}Ne might be even more deformed than ^{20}Ne although it is not so easy to position such a statement in the $\alpha \otimes {}^{16}\mathrm{O}/{}^{18}\mathrm{O}$ clusterization picture because of the modifications of the single-particle level scheme implied by the latter.

In terms of the geometry of our toy model, because we do not dispose with the mixing amplitudes it makes sense to consider only the case of ^{20}Ne, where there is an independent estimate [23] of $Q_0 = 53.6\ efm^2$. This value leads to estimates of $d_2 = 2.383$ fm and $d_1 = 2.014$. Therefore (see Fig. 11) the displacement of the two spheres is $\Delta = 0.37$ fm, i.e., about 14% of the radius of the bigger sphere (^{16}O). Such a small displacement seems quite reasonable and plausible.

V. CONCLUSIONS

New lifetime measurements using DSAM were carried out for ^{20,22}Ne to shed light on the problem of missing quadrupole collectivity in the transition strengths in the even-even Ne isotopes not reproduced without effective charges by shell model and configuration-mixing calculations. In ^{20}Ne, the lifetime of the 2_1^+ level was confirmed while in ^{22}Ne the analog lifetime was found to be shorter by 43%. The $B(E2)$ reduced transition strengths derived from these lifetimes as well as those for the heavier Ne isotopes are well described by involving mixing of α-cluster states of, e.g., the type $\alpha \otimes {}^{16}\mathrm{O}/{}^{18}\mathrm{O}$ with normal, nearly spherical states. The lifetime of the 4_1^+ state in ^{22}Ne also turned out to be shorter than the averaged value from the literature comprising 17 values measured between 1960 and 1984. The angular momentum dependence of the $B(E2)$ transition strengths between the yrast states in ^{20}Ne is well described by shell-model calculations starting from first principles, but other calculations for ^{22}Ne point to the necessity to improve the model descriptions.

ACKNOWLEDGMENTS

The authors are indebted to I. Ragnarsson for fruitful discussions. The support of the Romanian Ministry of Research and Innovation under under contract PN 18 09 01 02 NUCLEU Program is appreciated.

APPENDIX: CALCULATION OF THE QUADRUPOLE MOMENT OF TWO OVERLAPPING SPHERES

With the standard definition of the non-normalized intrinsic quadrupole moment in cylindrical coordinates via the integral

$$Q = 2\pi\left\{\int z^2 dz d\rho^2 - \int dz d\rho^4/4\right\} \tag{A1}$$

and with a coordinate system positioned at the center of charge of the system displayed in Fig. 11 the z axis being the axis of axial symmetry passing through the centers of the two spheres, one obtains:

$$\begin{aligned} Q = 2\pi\{ &-\left(R_2^2 - c^2\right)^2(d_2 + R_2)/4 - (c + R_2)^5/4 - 3c[(d_2 - c)^4 - (c + R_2)^4] + \left(\tfrac{3}{2}R_2^2 - \tfrac{5}{2}c^2\right)[(d_2 - c)^3 + (c + R_2)^3]/3 \\ &+c\left(R_2^2 - c^2\right)[(d_2 - c)^2 - (c + R_2)^2]/2 - \left(R_1^2 - a^2\right)^2(d_1 + R_1)/4 - (a + R_1)^5/4 + 3a[(a + R_1)^4 - (d_2 - c)^4 -] \\ &+\left(\tfrac{3}{2}R_1^2 - \tfrac{5}{2}a^2\right)[(a + R_1)^3 - (d_2 - c)^3]/3 - a\left(R_1^2 - a^2\right)[(a + R_1)^2 - (d_2 - c)^2 -]/2\}. \end{aligned} \tag{A2}$$

Here, $c = \frac{Z_1(d_2 - d_1)}{Z_1 + z_2}$ and $a = d_2 - d_1 - c$. We mention also that there is a relation interconnecting d_1 and d_2, namely

$$d_1 = \sqrt{R_1^2 - R_2^2 + d_2^2}. \tag{A3}$$

For normalization, one needs the volume integral, which reads:

$$V = \pi\left\{R_2^2(d_2+R_2)+R_1^2(d_1+R_1)-(c+R_2)^3/3-(a+R_1)^3/3-c((d_2-c)^2+c(c+R_2)^2)-c^2(d_2+R-2)-a(d_2-c)^2 \right.$$
$$\left. +a(a+R_1)^2-a^2(d_1+R_1)\right\}. \tag{A4}$$

Then, the intrinsic quadrupole moment can be calculated as

$$Q_0 = \frac{ZQ}{V} \tag{A5}$$

with the assumed homogeneous charge distribution ρ in the present work and $Z = Z_1 + Z_2$ being the total charge.

[1] P. Ring and P. Schuck, *The Nuclear Many-Body Problem* (Springer, Berlin, 1980).
[2] F. A. Majeed, *No-Core Shell Model Calculations for Some Light Nuclei* (Scholar's Press, Riga, 2015).
[3] G. C. Bonsignori, M. Bruno, A. Ventura, and D. Vretenar, *Hadrons, Nuclei and Applications* (Vol. 3) (World Scientific, Singapore, 2001).
[4] P. Petkov and C. Müller-Gatermann, Nucl. Instr. Meth. Phys. Res. A **915**, 40 (2019).
[5] A. E. Blaugrund, Nucl. Phys. **88**, 501 (1966).
[6] W. M. Currie, Nucl. Instr. Meth. **73**, 173 (1969).
[7] G. Winter, Nucl. Instr. Meth. **214**, 537 (1983).
[8] J. Le Bloas, N. Pillet, M. Dupuis, J. M. Daugas, L. M. Robledo, C. Robin, and V. G. Zelevinsky, Phys. Rev. C **89**, 011306(R) (2014).
[9] J. P. Elliott, Proc. Roy. Soc. (London) A **245**, 128 (1958).
[10] N. Tsunoda, T. Otsuka, N. Shimizu, M. Hjorth-Jensen, K. Takayanagi, and T. Suzuki, Phys. Rev. C **95**, 021304 (2017).
[11] G. K. Tobin, M. C. Ferriss, K. D. Launey, T. Dytrych, J. P. Draayer, A. C. Dreyfuss, and C. Bahri, Phys. Rev. C **89**, 034312 (2014).
[12] G. J. Fu, Y. M. Zhao, and A. Arima, Phys. Rev. C **90**, 054333 (2014).
[13] C. Robin, N. Pillet, M. Dupuis, J. Le Bloas, D. Pena Arteaga, and J.-F. Berger, Phys. Rev. C **95**, 044315 (2017).
[14] G. R. Jansen, M. D. Schuster, A. Signoracci, G. Hagen, and P. Navratil, Phys. Rev. C **94**, 011301 (2016).
[15] P. Marevic, J.-P. Ebran, E. Khan, T. Niksic, and D. Vretenar, Phys. Rev. C **97**, 024334 (2018).
[16] C. Beck, *Clusters in Nuclei* (Springer, Berlin, 2013), Vol. 3.
[17] M. Kimura, T. Suhara, and Y. Kanada-En'yo, Eur. Phys. J. A **52**, 373 (2016).
[18] A. Astier, P. Petkov, M.-G. Porquet, D. S. Delion, and P. Schuck, Phys. Rev. Lett. **104**, 042701 (2010).
[19] S. Ohkubo, Phys. Rev. Lett. **74**, 2176 (1995).
[20] Y. Suzuki and S. Ohkubo, Phys. Rev. C **82**, 041303(R) (2010).
[21] M. Spieker, S. Pascu, A. Zilges, and F. Iachello, Phys. Rev. Lett. **114**, 192504 (2015).
[22] P. Petkov, C. Müller-Gatermann, A. Dewald, A. Blazhev, C. Fransen, J. Jolie, P. Scholz, K. O. Zell, and A. Zilges, Phys. Rev. C **96**, 034326 (2017).
[23] F. Michel, G. Reidemeister, and S. Ohkubo, Phys. Rev. C **37**, 292 (1988).
[24] F. Michel, S. Ohkubo, and G. Reidemeister, Prog. Theor. Phys. Suppl. No. **132**, 7 (1998).
[25] P. Petkov, C. Müller-Gatermann, A. Dewald, A. Blazhev, C. Fransen, J. Jolie, P. Scholz, K. O. Zell, and A. Zilges, Phys. Rev. C **98**, 019904(E) (2018).
[26] H. Grawe and K. P. Lieb, Nucl. Phys. A **127**, 13 (1969).
[27] J. H. Anderso and R. C. Ritter, Nucl. Phys. A **128**, 305 (1969).
[28] R. J. Nickles, Nucl. Phys. A **134**, 308 (1969).
[29] G. Häusser, T. K. Alexander, A. B. McDonald, G. T. Ewan, and A. E. Litherland, Nucl. Phys. A **168**, 17 (1971).
[30] D. Schwalm, E. K. Warburton, and J. W. Olness, Nucl. Phys. A **293**, 425 (1977).
[31] K.-H. Speidel, P. N. Tandon, V. Mertens, W. Trölenberg, G. J. Kumbartzki, N. Ayres de Campos, M. M. Goldberd, J. Gerber, and M. Toulemonde, Nucl. Phys. A **378**, 130 (1982).
[32] K. W. Jones, A. Z. Schwarzschild, E. K. Warburton, and D. B. Fossan, Phys. Rev. **178**, 1773 (1969).
[33] D. R. Tilley, C. Cheves, J. Kelley, S. Raman, and H. Weller, Nucl. Phys. A **636**, 249 (1998).
[34] K. P. Lieb, Nucl. Phys. A **85**, 461 (1966).
[35] M. J. Throop, Phys. Rev. **179**, 1011 (1969).
[36] F. D. Snyder, Phys. Rev. C **6**, 204 (1972).
[37] R. L. Kozub, J. Lin, J. F. Mateja, C. J. Lister, D. J. Millener, J. W. Olness, and E. K. Warburton, Phys. Rev. C **27**, 158 (1983).
[38] N. Anyas-Weiss, R. Griffiths, N. A. Jelley, W. Randolph, J. Szucs, and T. K. Alexander, Nucl. Phys. A **201**, 513 (1973).
[39] D. C. Radford and A. R. Poletti, Nucl. Phys. A **275**, 141 (1977).
[40] M. Ogawa and E. Arai, J. Phys. Soc. Jap. **42**, 376 (1977).
[41] L. P. Ekstroem, D. E. C. Scherpenzeel, G. A. P. Engelbertink, H. J. M. Aaarts, and H. H. Eggenhuisen, Nucl. Phys. A **295**, 525 (1978).
[42] J. S. Forster, T. K. Alexander, G. C. Ball, W. G. Davies, I. V. Mitchell, and K. B. Winterborn, Nucl. Phys. A **313**, 397 (1979).
[43] T. K. Alexander, G. C. Ball, W. G. Davies, and J. S. Forster, Nucl. Phys. A **313**, 425 (1979).
[44] R. K. Bhalla and A. R. Poletti, Nucl. Phys. A **420**, 96 (1984).
[45] I. K. Fifield, J. Asher, and A. R. Poletti, J. Phys. G: Nucl. Phys. **4**, L65 (1978).
[46] L. D. Olivier, W. A. Richter, J. A. Stander, and J. W. Koen, Z. Phys. A **347**, 99 (1993).
[47] A. Dewald, O. Möller, and P. Petkov, Prog. Part. Nucl. Phys. **67**, 786 (2012)
[48] A. Dewald, S. Heinze, J. Jolie, A. Zilges, T. Dunai, J. Rethemeyer, M. Melles, M. Staubwasser, B. Kuczewski, J. Richter, U. Radtke, F. von Blanckenburg, and M. Klein, Nucl. Instr. Meth. Phys. Res. B **294**, 18 (2013)
[49] L. C. Northcliffe and R. F. Schilling, Nucl. Data Tables A **7**, 233 (1970).
[50] F. Ziegler, M. D. Ziegler, and J. P. Biersack, Nucl. Instr. Meth. Phys. Res. B **268**, 1818 (2010).
[51] G. Winter, ZfK Rossendorf Report ZfK-497, 1983.

[52] P. Petkov, J. Gableske, O. Vogel, A. Dewald, P. von Brentano, R. Krücken, R. Peusquens, N. Nicolay, A. Gizon, J. Gizon, D. Bazzacco, C. Rossi-Alvarez, S. Lunardi, P. Pavan, D. R. Napoli, and W. Andrejtscheff, and R. V. Jolos, Nucl. Phys. A **640**, 293 (1998).
[53] J. Lindhard, M. Scharff, and H. E. Schiøtt, Kgl. Dan. Vid. Selsk. Mat. Fys. Medd. **33**, 1 (1963).
[54] J. F. Ziegler and J. P. Biersack, in *Treatise on Heavy-Ion Science*, Vol. 6, edited by D. A. Bromley (Plenum Press, Berlin, 1985), p. 95.
[55] J. Keinonen, Capture gamma-ray spectroscopy and related topics-1984, in *Proceedings of the Fifth International Symposium, Knoxville, Tennessee*, edited by S. Raman, AIP Conf. Proc. No. 125 (AIP, New York, 1985), p. 557.
[56] T. K. Alexander and J. S. Forster, Adv. Nucl. Phys. **10**, 197 (1978).
[57] P. Petkov, D. Tonev, J. Gableske, A. Dewald, and P. von Brentano, Nucl. Instr. Meth. Phys. Res. A **437**, 274 (1999).
[58] P. Petkov, A. Dewald, D. Tonev, N. Goutev, G. Asova, B. Dimitrov, G. Gavrilov, M. N. Mineva, and M. S. Yavahchova, Nucl. Instr. Meth. Phys. Res. A **783**, 6 (2015)
[59] P. Petkov, AIP Advances **8**, 075305 (2018).
[60] G. Boehm, A. Dewald, P. Petkov, and P. von Brentano, Nucl. Instr. Meth. Phys. Res. A **329**, 248 (1993).
[61] D. K. Olsen, A. R. Barnett, S. F. Biagi, N. H. Merrill, and W. R. Phillips, Nucl. Phys. A **220**, 541 (1974).
[62] X. K. Maruyama, F. J. Kline, J. W. Lightbody, S. Penner, W. J. Briscoe, M. Lunnon, and H. Crannell, Phys. Rev. C **19**, 1624 (1979).
[63] P. Petkov, M. Yavahchova, D. Tonev, N. Goutev, and A. Dewald, Nucl. Instrum. Methods Phys. Res. A **711**, 96 (2013).
[64] P. Petkov *et al.*, Phys. Rev. C **68**, 034328 (2003).
[65] A. Dewald, S. Harissopulos, and P. von Brentano, Z. Phys. A **334**, 163 (1989).
[66] M. S. Basunia, Nucl. Data Sheets **127**, 69 (2015).
[67] I. Ragnarsson (private communication).
[68] K. Arnswald *et al.*, Phys. Lett. B **772**, 599 (2017).
[69] R. B. Firestone, Nucl. Data Sheets **108**, 2319 (2007).
[70] M. S. Basunia and A. M. Hurst, Nucl. Data Sheets **134**, 1 (2016).
[71] M. S. Basunia, Nucl. Data Sheets **114**, 1189 (2013).